Fluorescence lifetime enables high-resolution analysis of neuromodulator dynamics across time and animals

Pingchuan Ma[1,2], Peter Chen[1,3], Elizabeth Tilden[1,2], Samarth Aggarwal[1], Anna Oldenborg[1], and Yao Chen[1, †]

1. Department of Neuroscience, Washington University in St. Louis, St. Louis, MO 63110
2. Ph.D. Program in Neuroscience, Washington University in St. Louis
3. Master's Program in Biomedical Engineering, Washington University in St. Louis

[†]Correspondence: yaochen@wustl.edu

ABSTRACT

Optical sensors have transformed the field of neuromodulation because neuromodulator dynamics are essential for their function. Despite their high spatial and temporal resolution, these fluorescence intensity-based sensors are sensitive to sensor expression level and excitation light fluctuation, thus preventing analysis of neuromodulators across time or animals. Here, we screened neuromodulator sensors and discovered that multiple sensors showed response in fluorescence lifetime, a property independent of sensor expression or excitation light power. The acetylcholine sensor GRAB-ACh3.0 showed the largest lifetime change. Fluorescence lifetime of GRAB-ACh3.0 responds to transient ACh release, is dose sensitive, and is insensitive to excitation laser power. In mice across sleep/wake and running/resting states, fluorescence lifetime, in contrast to intensity, predicts behavior states accurately despite change in sensor expression level across weeks and animals. Thus, fluorescence lifetime of neuromodulator sensors enables comparison of neuromodulator dynamics at high resolution across different animals, brain regions, disease models, and chronic time scales.

KEYWORDS

Optical sensors, neuromodulator, fluorescence lifetime, acetylcholine, sleep, running, behavior states, high-resolution dynamics, chronic, tonic

INTRODUCTION

Neuromodulators such as acetylcholine and dopamine can reconfigure circuits and transform animal behaviors (Bargmann and Marder, 2013; Marder, 2012). They play important roles for normal physiology and their mis-regulation is implicated in many neurological and psychiatric disorders. The location and timing of neuromodulator release are critical to determine neuromodulator functions, but capturing neuromodulator dynamics with high spatial and temporal resolution was challenging. Classical methods such as microdialysis, fast-scan cyclic voltammetry, or electrophysiology recordings of putative neurons that release neuromodulators provided great insights (Arbuthnott and Wickens, 2007; Ganesana et al., 2017; Puthongkham et al.; Sabatini and Tian, 2020; Tuveson et al., 2004; Ungerstedt et al.; Venton et al.; Watabe-Uchida et al., 2017; Wightman, 2006), but lacked in spatial and temporal resolution suited for behavior, specific targeting to cells of interest, or selectivity. Recently, genetically encoded optical reporters of neuromodulators are transforming the field because they can be targeted to cells of interest, have the same spatial resolution as optical microscopy, and the temporal resolution is suited for animal behavior (Dong et al., 2022; Sabatini and Tian, 2020; Wu et al., 2022).

Fluorescence intensity-based optical biosensors have provided valuable information on how fast neuromodulator transients correlate with animal behavior, but these sensors are also sensitive to sensor expression level and excitation light fluctuation. These limitations are not easily overcome by including a second fluorophore that does not change with neuromodulator concentration for normalization purpose, because the rate of expression level change, bleaching, and optical scattering are often different between different fluorophores. Thus, fluorescence intensity-based biosensors cannot be used to compare neuromodulator release between different animals, between different time points, between control and disease/perturbation conditions, or quantitate changes in tonic levels of neuromodulators. These changes are nevertheless essential to understand behavior. For example, tonic, but not phasic increase of firing of norepinephrine neurons are sufficient for anxiety-like and averse behavior (McCall et al., 2015). Tonic versus phasic cannabinoid receptor activity regulates synaptic transmission and plasticity via diverse mechanisms (Jensen et al., 2021). Tonic dopamine levels prior to stimulus delivery are predictive of upcoming hallucination-like percepts (Schmack et al., 2021). Thus, an ideal neuromodulator sensor would combine the benefits of microdialysis and fluorescence intensity-based sensors to allow measurement of neuromodulator concentrations both at high spatial and temporal resolution, and across animals and long time scales.

Fluorescence lifetime imaging microscopy (FLIM) could be ideal for chronic imaging at high spatial and temporal resolution. Because fluorescence lifetime measure the time between excitation and light emission of a fluorophore, this intensive property is independent of sensor expression level or fluctuation in excitation light power (Becker and Bergmann, 2002; Chen and Sabatini, 2012; Yasuda, 2006), both of which happen during chronic imaging. Most FLIM sensors involve dyes or are based on Förster Resonance Energy Transfer (FRET) (Chen et al., 2014; Lakowicz et al., 1992; Lazzari-Dean et al., 2019; Yasuda, 2006; Zheng et al., 2015, 2018). Although there are a few examples of single-fluorophore protein-based sensors (Brinks et al., 2015; van der Linden et al., 2021; Mongeon et al., 2016), they are rarer, and it is hard to predict whether

a given sensor will show fluorescence lifetime change. Thus, it is unclear whether single fluorophore-based neuromodulator sensors can display fluorescence lifetime change and whether FLIM imaging can be used to predict neuromodulator levels across animals and across long time.

Here, we screened existing neuromodulator sensors (Borden et al., 2020; Feng et al., 2019; Jing et al., 2018, 2020; Patriarchi et al., 2018; Sun et al., 2020; Wan et al., 2021) and found fluorescence lifetime response in a small fraction of them. Notably, we found the largest fluorescence lifetime change in GRAB-ACh3.0 (GPCR-Activation-Based-Acetylcholine) (Jing et al., 2020). Importantly, this lifetime change is authentic and is not simply due to the relative intensity increase of GRAB-ACh3.0 relative to autofluorescence. FLIM measurement of GRAB-ACh3.0 can detect transient ACh changes, is dose sensitive, insensitive to excitation laser power fluctuation, and shows high reproducibility within a cell. In vivo, we measured both fluorescence lifetime and fluorescence intensity of GRAB-ACh3.0 with photometry in behaving mice under different sleep/wake or running/resting states. We found that fluorescence lifetime is a much better predictor of behavior states than intensity, especially across varying laser powers, across weeks, and across animals. The discovery and characterization of fluorescence lifetime change of a single fluorophore-based neuromodulator sensor enables the exploration of previously unknown biological questions – it allows monitoring of both phasic and tonic changes, both chronic and transient changes, and both across animal and within animal changes of neuromodulators. Furthermore, these results open doors to convert many fluorescence intensity-based neuromodulator sensors into lifetime-based sensors that enable analysis of neuromodulators across animals, conditions, locations, and chronic time scales.

RESULTS

Fluorescence Lifetime Changes of Neuromodulator Sensors

We set out to test whether any existing intensity-based neuromodulator sensors also showed a fluorescence lifetime change (Fig. 1A). We expressed individual sensors in human embryonic kidney (HEK) 293T cells and imaged sensor fluorescence with two-photon fluorescence lifetime imaging microscopy (2pFLIM). Surprisingly, in addition to fluorescence intensity changes that were reported previously, multiple sensors showed significant fluorescence lifetime increase in response to saturating concentrations of the corresponding neuromodulators (Fig. 1B). The acetylcholine (ACh) sensor GRAB-ACh3.0 (Jing et al., 2020) showed the largest fluorescence lifetime change of 0.18 ns±0.01 ns in response to 100 μM ACh ($n = 13$, $p < 0.0001$) (Fig. 1B and 1C). In fact, the fluorescence lifetime change paralleled intensity change of the ACh sensor (Fig. 1D-1I). In control experiments, both lifetime and intensity change were reversed by the muscarinic receptor antagonist tiotropium (Tio, 5 μM, Fig. 1D-I, $n = 13$, $p < 0.0001$). Furthermore, the mutant sensor GRAB-ACh3.0Mut did not show any intensity or fluorescence lifetime change in response to ACh (Fig. S1). These results indicate that single fluorophore-based neuromodulator sensors can show fluorescence lifetime responses.

We next examined whether the fluorescence lifetime change we measured truly reflected fluorescence lifetime change of GRAB-ACh3.0. The fluorescence lifetime measured in HEK 293T cells is contributed by both the fluorescent sensor and autofluorescence. In fact, it is a weighted

average of sensor lifetime and autofluorescence lifetime, weighted by their relative intensity (Fig. 2A). Autofluorescence displays a shorter fluorescence lifetime than green fluorescent proteins (Fig. 2B). Therefore, even if a biosensor did not show lifetime change, its intensity increase in response to a neuromodulator would result in an increase of measured fluorescence lifetime, because of the increase in weight in the weighted average (Fig. 2A). Thus, we performed computational simulation to test whether the fluorescence lifetime change we observed could be simply explained by intensity change. For the simulation, we used measured autofluorescence and realistic GRAB-ACh3.0 fluorescence intensity changes between 0 and 100 μM ACh, and sampled from populations of photons (Fig. S2). Our simulation showed that if the sensor itself did not show any fluorescence lifetime increase, its intensity increase only caused a small increase of overall fluorescence lifetime (Fig. 2C, 0.007 ns, n = 50). In contrast, the experimentally measured lifetime increase in response to 100 μM ACh was much larger (Fig. 2C, 0.13 ns). Thus, the observed fluorescence lifetime change in cells expressing GRAB-ACh3.0 is not solely due to an increase in fluorescence intensity. GRAB-ACh3.0 sensor itself responds to ACh with authentic fluorescence lifetime increase.

Fluorescence lifetime of ACh sensor is dose-dependent and detects ACh transient in the brain

For fluorescence lifetime measurement of GRAB-ACh3.0 to be useful in biological applications, it needs to be sensitive enough to show dose-dependent responses to ACh and to detect transient release of ACh in the brain. In response to different concentrations of ACh ranging from 1 nM to 100 μM, both fluorescence lifetime and intensity of GRAB-ACh3.0 in HEK cells showed dose-dependent increase. In response to each new concentration of ACh, fluorescence intensity showed an initial increase followed by a decrease (Fig. 3A). In contrast, fluorescence lifetime was stable given a certain concentration of ACh (Fig. 3A). Thus, these results show stable fluorescence lifetime response of GRAB-ACh3.0 to different concentrations of ACh.

In order to test whether fluorescence lifetime of GRAB-ACh3.0 can report ACh levels in brain tissue, we delivered the reporter via adeno-associated virus injection to the hippocampus (Fig. 3B). ACh (1 μM and 100 μM) induced dose-dependent response in the fluorescence lifetime of the ACh sensor (Fig. 3C, 3D; n = 9; 0.073 ns ± 0.015 ns, p = 0.054 (1 μM ACh); 0.13 ns ± 0.022 ns, p < 0.0001 (100 μM)), indicating that fluorescence lifetime of GRAB-ACh3.0 is sensitive enough to report ACh concentration ex vivo.

In order to mimic transient ACh release in vivo, we puffed ACh (200 μM) onto the soma of CA1 pyramidal neurons (Fig. 3E), at temporal duration (3 seconds) comparable to ACh release measured in behaving mice (Parikh et al., 2007). Fluorescence lifetime of GRAB-ACh3.0 increased transiently in response to 3s of ACh delivery (Fig. 3F, 3G; n = 11, 0.125 ± 0.017 ns). Thus, fluorescence lifetime of GRAB-ACh3.0 can report transient ACh release in brain tissue.

Fluorescence lifetime of ACh sensor is independent of laser power and is consistent within a cell

Fluorescence lifetime should be independent of laser power fluctuation, less sensitive to sensor internalization, and is independent of sensor expression levels. Thus, we set out to measure both fluorescence lifetime and intensity under these circumstances, in order to explore the extent of

these advantages. We first imaged cells with different laser excitation powers. Fluorescence lifetime of the ACh sensor was stable across different laser powers (Fig. 4A, 4C). As a result, fluorescence lifetime showed statistically significant separation between baseline and high ACh conditions despite different laser powers (Fig. 4C; $n = 15$, $p < 0.0001$). In fact, 80.49% of the variance of sensor lifetime can be explained by ACh concentration, with very minimal contribution from laser power (0.57%) or cell identity (9.30%, Fig. 4C). In contrast, with varying laser power, fluorescence intensity of GRAB-ACh3.0 varied greatly (Fig. 4A, 4B). As a result, the absolute fluorescence intensity has little predictive value for ACh concentration, with only 30.25% of sensor intensity variance explained by ACh concentrations (Fig. 4B). These results indicate that fluorescence lifetime is a more reliable measurement of ACh concentration than fluorescence intensity under fluctuating laser powers.

In order to use the absolute fluorescence lifetime value to predict ACh concentrations, lifetime would also need to be stable within a cell for a given ACh concentration. We therefore repeatedly applied ACh (1 μM) to the same cell and measured fluorescence intensity and lifetime. Fluorescence lifetime in response to the same concentration of ACh was consistent within a cell across repeated application (Fig. S4; $n = 17$, $p = 0.46$). Thus, lifetime is a consistent measure of ACh concentration within a cell.

Taken together, fluorescence lifetime measurement of GRAB-ACh3.0 is consistent with fluctuating laser excitation power and is consistent with repeated ACh application within a cell.

Fluorescence lifetime predicts neuromodulator and behavior states with high accuracy across imaging conditions, across weeks, and across mice

Fluorescence Lifetime Photometry (FLiP) measures the bulk fluorescence from a population of cells surrounding the tip of the fiber implant, thus allowing for the measurement of neuromodulator dynamics in vivo in a given region (Lee et al., 2019). The signal-to-noise ratio for the bulk signal is even higher than methods with cellular resolution. In fact, the variance of the signal is inversely correlated with the number of cells. Thus, if the bulk signal of ~1000 cells were analyzed, the standard deviation of lifetime distribution would be $\frac{1}{\sqrt{1000}} \sim \frac{1}{32}$ of the standard deviation across single cells (Fig. S5A), making fluorescence lifetime photometry a superb method to measure ACh level in vivo.

Our ultimate goal is to compare ACh levels across imaging conditions, mice, and weeks at high temporal resolution. Intensity measurement can only reflect the acute transition between behavior states, whereas fluorescence lifetime provides the possibility of predicting the absolute level of ACh that is correlated with the behavior state of animals at any given point in time. To test if this is possible, we conducted proof-of-principle experiments to ask if absolute fluorescence lifetime of GRAB-ACh3.0 can predict ACh concentration due to different behavior states, across varying laser powers, mice, and sensor expression levels.

First, we tested whether fluorescence lifetime measurement of the ACh sensor correlates with running versus resting (Jing et al., 2020) regardless of excitation laser power or mouse identity

(Fig. 5, S5). This mimics realistic scenarios in sensor application because fluctuating laser power can arise from unstable laser source, environmental changes, or movement artifacts.

Remarkably, lifetime measurement was consistent for a given behavior state even across different excitation laser powers (Fig. 5C) and across mice (Fig. 5D). Furthermore, lifetime measurement showed significant increase from resting to running, even when results with different laser powers and from different mice are combined (Fig 5E; n = 326 (resting) vs 465 (running), $p < 0.0001$). In contrast, fluorescence intensity, is not statistically different between running and resting when different imaging conditions are combined (Fig. 5E; n = 326 (resting) vs 465 (running), $p = 0.44$). Quantitatively, most of the variance in lifetime is explained by behavior state (65.74%), with small contribution from the variance of laser power (13.03%) and animal identity (4.21%) (Fig. 5F; stepwise generalized linear model (GLM)). In contrast, the majority of the variance in intensity is explained by animal identity (65.71%), followed by the laser (24.27%), with <2.68% explained by behavior state. Consistent with the above analyses, when we asked conversely how accurately can we predict running versus resting states based on lifetime or intensity, absolute lifetime showed much higher prediction accuracy than intensity (F1=0.92 for lifetime, F1= 0.62 for intensity; multinomial logistical regression (MLR)) (Fig. 5G). These results indicate that fluorescence lifetime is more reliable and has more predictive power than intensity to estimate behavior state with fluctuating laser powers across animals.

In vivo, fluorescent sensor often varies in expression level over time and across animals. We thus investigated whether fluorescence lifetime can accurately track ACh levels over many weeks, even as sensor expression level increases. We used the sleep-wake cycle of mice as our proof-of-principle experimental setup because hippocampal ACh is known to be high during active wake (AW) and Rapid Eye Movement (REM) phase of sleep, and low during quiet wakefulness (QW) and Non-REM (NREM) phase of sleep (Jing et al., 2020). To test whether fluorescence lifetime measurement is advantageous over intensity across time and animals, we monitored ACh sensor with FLiP, while simultaneously performing EEG/EMG/video recordings to identify sleep-wake stages (Fig. 6A).

Within one 12-hour recording for a given mouse, both fluorescence lifetime and intensity of GRAB-ACh3.0 showed an increase during AW and REM and a decrease during QW and NREM (Fig. 6B, 6C; n=69, 28, 54, 16 epochs for AW, QW, NREM, and REM, $p < 0.0001$). Unexpectedly, mutant ACh sensor that does not bind to ACh showed a decrease in fluorescence intensity, but not lifetime, as the mice transited into REM sleep (Fig S6). These results indicate that that fluorescence lifetime, like intensity (Jing et al., 2020), can distinguish ACh levels across different sleep/wake stages; fluorescence lifetime, unlike intensity, is resistant to environment changes.

How does fluorescence lifetime compare with intensity as sensor expression level increases over time? Strikingly, fluorescence lifetime remained stable at a given behavioral state, even as sensor expression changed over time (Fig. 6D, 6E). 60% (63.34% ± 6.61%) of the variation in fluorescence lifetime can be explained by variation in behavior states, and only ~10% (11.50% ± 6.01%) is due to sensor expression time (Fig. 6E, two-way ANOVA). In contrast, fluorescence intensity showed drastic changes over time (Fig. 6D, 6E). Only 10% (10.05% ± 4.09%) of the variability of fluorescence intensity can be explained by NREM/REM states, whereas 70% (70.41%

± 5.37%) of the variability is due to the amount of sensor expression time (Fig. 6E, two-way ANOVA). Together, these results indicate that fluorescence lifetime, compared with intensity, is a better measurement of ACh concentrations, as sensor expression changes over days and weeks.

Next, we compared lifetime versus intensity measurement across different mice. Behavior state contributed more to lifetime variance than animal identity, whereas the variance of intensity was mostly explained by animal identity, likely reflecting on different sensor expression levels across mice (Fig. 6F; two-away ANOVA). If we combine behavior states, time, and animal identity together, lifetime variance was mostly explained by NREM versus REM states (49.98%), whereas fluorescence intensity was largely explained by animal identity (58.54%), followed by sensor expression time (22.85%), with minimal contribution from behavior states (1.46%) (Fig. 6G; step-wise GLM). Therefore, fluorescence lifetime is a better correlate of behavior states than intensity, when data from multiple animals need to be considered.

Finally, we asked how accurately lifetime or intensity could predict behavior states. Lifetime predicted NREM versus REM states with much higher accuracy than intensity, despite changing expression level and different animals (F1 = 0.85 for lifetime, F1 = 0.6 for intensity, MLR) (Fig. 6H).

Taken together, these results indicate that in vivo, fluorescence lifetime accomplishes what fluorescence intensity measurement cannot do: it predicts behavior states with high accuracy with little sensitivity to excitation light, environmental changes, sensor expression, and across animals.

DISCUSSION

In order to measure neuromodulator levels at high temporal resolution and make comparison across days and across animals, we investigated whether optical sensors for neuromodulators may show a fluorescence lifetime change. We discovered fluorescence lifetime response for multiple neuromodulator sensors. Similar to fluorescence intensity, lifetime measurement allows detection of transient neuromodulator changes and is dose sensitive. In contrast to fluorescence intensity, fluorescence lifetime is insensitive to excitation laser power fluctuation and shows high reproducibility within a cell. In vivo, fluorescence lifetime is a much better correlate of behavior states than fluorescence intensity, especially across days and across animals as sensor expression level changes. Thus, fluorescence lifetime measurement of neuromodulator sensors opens doors to study neuromodulator dynamics at high spatial and temporal resolution, and across animals, locations, and chronic time scale.

Using fluorescence lifetime to measure neuromodulator concentrations

The most important advantage of fluorescence lifetime comes from the measurement of an intensive property of the sensor that is independent of sensor expression (Becker and Bergmann, 2002; Chen and Sabatini, 2012; Yasuda, 2006). Thus, fluorescence lifetime of neuromodulator sensors is robust with animal movement, across animals (Fig. 5 and 6), with changing sensor expression levels over time (Fig. 6), and with fluctuating excitation light power (Fig. 4 and 5). In addition, in response to the same neuromodulator concentration, intensity measurement showed decreased fluorescence intensity over time, whereas fluorescence lifetime showed stable response

(Fig. 2A). The changing intensity response may be due to sensor internalization that makes ACh unable to reach the sensor, which would result in lower intensity but unaltered lifetime. Thus, fluorescence lifetime measurement may be advantageous over intensity measurement when the biosensor undergoes internalization, or when the study compares between conditions of fluctuating excitation light powers or varying sensor expression levels.

Should we always use fluorescence lifetime measurement rather than fluorescence intensity? Because accurate lifetime measurement requires many photons, the temporal resolution is not as short as can be achieved by fluorescence intensity. For a reasonable signal/noise ratio, hundreds of milliseconds are needed for each lifetime measurement. This temporal resolution is not a significant compromise for neuromodulator measurement since most neuromodulator sensors have an off rate that is similar in magnitude. This subsecond temporal resolution is far greater than microdialysis, which can be used to compare between animals and across longer time scale. Therefore, fluorescence lifetime measurement with optical sensors combines the advantages of fluorescence intensity measurement and microdialysis, enabling high spatial and temporal resolution analysis of neuromodulator dynamics and allowing comparison across time and animals.

Practical considerations of lifetime imaging of neuromodulator sensors

The ideal fluorescence lifetime-based neuromodulator sensor has high signal-to-noise ratio, distinguishing different neuromodulator concentrations with high sensitivity and reporting the same neuromodulator concentrations with consistent lifetime readout. Fluorescence lifetime photometry (FLiP) experiments report GRAB-ACh3.0 lifetime from ~100 to ~1000 cells, thus reducing the standard deviation of lifetime distribution at a given behavior state by 10 to 30-fold. Thus, as demonstrated by our results, fluorescence lifetime measurement of GRAB-ACh3.0 shows high signal-to-noise ratio and clear separation of behavior states (Figs. 5 and 6).

Mutant sensor controls are essential for the correct interpretation of results for any experiments using biosensors. Here, consistent with previous reports (Jing et al., 2020), we found an increase in ACh during REM sleep, demonstrated by the increase of both fluorescence intensity and lifetime of GRAB-ACh3.0 (Fig. 6). Surprisingly, we observed a decrease in fluorescence intensity during REM sleep with a mutant ACh sensor that does not bind to ACh (Fig. S6). Thus, this intensity decrease was not due to ACh. Interestingly, fluorescence lifetime measurement of the mutant sensor did not show a decrease during REM sleep compared with other behavior states (Fig. S6). These results suggest that the REM-associated intensity decrease in the mutant sensor was not due to a change in quantum efficiency, but a change in photon absorption by the fluorophore, potentially due to REM-associated hemodynamic changes. This REM-associated intensity decrease was similar to what was observed with the wild type version of other neuromodulator sensors, calling for careful interpretation of data to avoid potential confound. This fluorophore intensity change,unrelated to neuromodulators, therefore demonstrates that fluorescence lifetime is more robust in the presence of environmental changes that can alter photon absorption.

Opportunities for new biology and for new sensors

The discovery and demonstration of the biological utility of fluorescence lifetime-based sensors opens new opportunities for biological discovery. As demonstrated in our proof-of-principle

results with sleep-wake stages and running-resting states (Fig. 5 and 6), lifetime measurement is insensitive to sensor expression change over time, laser light fluctuation, and sensor expression differences across mice. As a result, lifetime measurement of optical sensors reflects neuromodulator concentrations, and the absolute lifetime is a much better predictor of behavior states than intensity (Fig. 5 and 6). Since intensity measurement could not be used to make comparison between conditions where sensor expression level may differ, lifetime measurement of neuromodulator sensors provide unique opportunities to uncover new biology of changes in tonic levels of neuromodulators, changes of neuromodulators across days, across animals, across brain regions, and between wild type and disease models.

In addition to the significance to biology, our discovery of lifetime change by single fluorophore-based GPCR neuromodulator sensors provides a beginning of evolving more lifetime-based neuromodulator sensors. Future endeavors will be applied to evolve sensors with only fluorescence intensity change into lifetime-based sensors and evolving sensors with larger dynamic range in fluorescence lifetime.

Taken together, we discovered, characterized, and demonstrated the utility of fluorescence lifetime changes of neuromodulator sensors. Fluorescence lifetime measurement can reveal previously unavailable information on neuromodulator dynamics across brain regions, days, and animals at high spatial and temporal resolution. This opens possibilities to reveal new biology of neuromodulator dynamics in cells, brain tissue, and animals.

METHODS

HEK293T Cells

HEK 293T cells were cultured in DMEM with 10% FBS (Millipore Sigma), GlutaMAX (Invitrogen), and penicillin /streptavidin ((50 U/m, Corning) at 37℃ in 5% CO2. The gender of the cells is female. The cell line has not been authenticated. The cells were used to characterize the fluorescence lifetime changes of the neuromodulator sensors using two-photon fluorescence lifetime imaging. They were plated on coverslips in 24-well plates and transfected with plasmids using lipofectamine 2000 (Invitrogen). Two days after transfection, the cells were imaged with artificial cerebrospinal fluoid (ACSF, concentrations in mM: 127 NaCl, 25 Na2CO3, 1.25 NaH2PO4.H2O, 2.5 KCl, 1 MgCl2, 2 CaCl2, and 25 glucose) perfusion.

Animals

C57BL/6 mice were used in this study. All procedures for rodent husbandry and surgery were performed following protocols approved by the Washington University Institutional Animal Care and Use Committee and in accordance with National Institutes of Health guidelines. For acute brain slices, wild-type mice (from Jackson Laboratory) were used with injections of virus expressing Cre recombinase and Cre-dependent sensors. For behavioral studies, Emx1-IRES-Cre (Jax 005628) mice were used with injections of Cre-dependent ACh 3.0 virus (AAV9-hSyn-DIO-ACh3.0) and optic fiber, EEG/EMG, and headplate implants.

DNA plasmids

The constructs pdisplay-CMV-ACh-3.0, pdisplay-CMV-5HT3.5, pdisplay-CMV-NE3.1, pdisplay-gACh3.0-mutant, and pdisplay-DA2h were gifts from Dr. Yulong Li's laboratory (Feng et al., 2019; Jing et al., 2020; Sun et al., 2020; Wan et al., 2021). pAAV-CAG-dLight1.1 (Addgene #111067) was made in Dr. Lin Tian's laboratory (Patriarchi et al., 2018). iAChSnFR (Addgene #137955) was made in Dr. Loren Looger's laboratory (Borden et al., 2020).

Virus Production and Stereotaxic Injections

The AAV9-hSyn-DIO-ACh-3.0 was packaged at Vigene Biosciences or WZ Biosciences with the permission of Dr. Yulong Li. AAV5-CamKII-Cre was purchased from Addgene (#105558). For stereotaxic injection, the dorsal hippocampus CA1 was targeted with coordinates of posterior 1.78 mm and lateral 1.58 mm relative to Bregma, 1.36 mm from the pia. All injections were made at a rate of 100 nL/min through a UMP3 micro-syringe pump (World Precision Instruments) via glass pipette. For acute brain slice imaging, bilateral injections of 500 nL of AAV9-hSyn-DIO-Ach-3.0 and AAV5-CamKII-Cre mix (at 4:1 ratio) were made in wild-type mice. For fluorescence lifetime photometry experiments, unilateral injections of 500 nL of AAV9-hSyn-DIO-ACh-3.0 were made into the left hemispheres of Emx1-IRES-Cre mice, followed by optic fiber, EEG/EMG implants, and headplate implantations.

Implantation of optic fiber, EEG/EMG implants, and headplate

After stereotaxic injection and withdrawal of the glass pipette, an optic fiber (Doric Lenses, B280-2101-2.5) was inserted into the same injection site, at 0.1 mm above the viral injection site. The fiber was stabilized to the skull with glue. To implant the EEG and EMG implants, four stainless screws were inserted into the skull, with two above the cerebellum, one above the right hippocampus, and one above the right frontal cortex. The screws were wired to an EEG/EMG head-mount (Pinnacle 8402). Two EMG electrodes from the head-mount were inserted into the neck muscle of the mice. A headplate was placed directly onto the skull. All the implants were secured to the skull with dental cement. Additional layer of dental cement with black paint was applied for light-proofing. All experiments were carried out at least 2 weeks after the surgery.

Acute Brain Slice Preparation

Mice were anesthetized with isoflurane before intracardial perfusion with cold NMDG-based cutting solution (concentrations in mM: 93 NMDG, 2.5 KCl, 1.2 NaH2PO4, 30 NaHCO3, 20 HEPES, 25 glucose, 10 MgSO4, 0.5 CaCl2, 5 sodium ascorbate, 2 thiourea, and 3 sodium pyruvate) (Ting et al., 2018). Their brains were rapidly dissected out. 300 μm-thick coronal sections were obtained with a Leica VT1000S vibratome (Leica Instruments) in cold NMDG-based cutting solution. After sectioning, slices were transferred to NMDG-based solution and incubated at 34 ℃ for 12 minutes, and then kept in HEPES-based holding solution (concentrations in mM: 92 NaCl, 2.5 KCl, 1.25 NaH2PO4, 30 NaHCO3, 20 HEPES, 2 thiorea, 5 sodium ascorbate, 3 sodium pyruvate, 2 CaCl2, 2 MgSO4, and 25 gluocose) at room temperature with 5% CO2 and 95% O2. Slices were then transferred to a microscope chamber and ACSF was perfused at a flow rate of 2-4 mL/min.

Two-photon Fluorescence Lifetime Imaging (2pFLIM) and image analysis

Two photon imaging was achieved by a custom-built microscope with a mode-locked laser source (Insight X3, 80 MHz, Spectra-Physics). Photons were collected with fast photomultiplier tubes (PMTs) (H10770PB-40, Hamamatsu). A 60X (NA1.1) objective (Olympus) was used. Image acquisition was performed using a custom-written software ScanImage that ran in MATLAB 2012b (Pologruto et al., 2003).

FLIM was performed as described previously (Chen et al., 2014, 2017). For all the GFP-based neuromodulator sensors, 920 nm was used as the excitation wavelength. Emission light was collected through a dichroic mirro (FF580-FDi01-25X36, Semrock) and a band-pass filter (FF03-525/50-25, Semrock). 128x128 pixel images were collected by frame scan at 4 Hz. The FLIM board SPC-150 (Becker and Hickl GmbH) was used, and time-domain single photon counting was performed in 256 time channels. Fluorescence lifetime of the neuromodulator sensor was calculated empirically based on regions of interest (ROI) of the cells. After image registration, the membrane of individual cells was selected as ROI. Photons from all the effective pixels of a given ROI were pooled to generate the 256-channel histogram. The average photon count per pixel was used as a measurement of intensity. The empirical fluorescence lifetime (see calculation below in FLiP analysis) was of ACh 3.0 in the corresponding ROI was calculated.

The amplitudes of lifetime changes were quantitated as follows:

BaselineStart = lifetime measurements averaged over the first minute of baseline;

BaselineEnd = lifetime measurements averaged over the last minute of baseline;

BaselineMax = maximum lifetime measurement during baseline;

TreatmentMax = maximum lifetime measurement after a treatment;

Δlifetime (baseline) = BaselineMax - BaselineStart;

Δlifetime (Treatment) = TreatmentMax – BaselineEnd.

Fluorescence Lifetime Photometry (FLiP) and Analysis

A custom-built fluorescence lifetime photometry setup was built and used similar to previously described (Lee et al., 2019). In brief, a pulsed 473nm laser (BDS-473-SM-FBE Becker and Hickl (BH) operating at 50 MHz) was used as the excitation light source. An optical fiber patch cord was used to direct excitation laser beam to the optical fiber implanted in the mouse brain. A dichroic mirror and band-pass filter was used to select the green emission light from the blue excitation light Emission light was detected with a fast photomultiplier tube (PMT, H10770PA-40-Y007, HamamatsuSPC-150(BH), a time-correlated single-photon counting (TCSPC) board was used to measure fluorescence lifetime. The data were collected by custom software in MATLAB 2012b, which calculated the average lifetime of detected photons at 1s intervals. Photon arrival rate was adjusted to be between 1x10^5/s and 8x20^6/s for accurate estimation of lifetime while under the upper limit imposed by the TCSPC driver board. The typical excitation power needed to generate the appropriate rate of photons (about 300 kHz) for TCSPC was about 0.01–0.18 μW (measured at the output end of the patch cord).

We calculated the average empirical fluorescence lifetime of a given acquisition as follows.

$$\tau = \frac{\sum F(t) * t}{\sum F(t)}$$

in which F(t) is the photon count from the fluorescence lifetime histogram at time bin t, t is the lifetime measurement corresponding to the time bin. We performed the calculation between 0.0489ns to 12 ns in the lifetime histogram.

FLiP, EEG/EMG, and Video Recordings

Mice that underwent ACh 3.0 virus injection, optical fiber implantation, and EEG/EMG implant were placed in a chamber with 12-hour/12-hour light-dark cycle (6am-6pm light). An additional infrared light was used for video recording during the dark phase. Fluorescence lifetime data were collected at 1Hz with our custom-built FLiP setup. EEG/EMG recording was performed at 400 Hz with a system from Pinnacle Technology using our ScanImage software. Video recording was performed at 25 Hz with a camera using the software Bonsai (https://bonsai-rx.org/). Video data were synchronized with FLiP and EEG/EMG data via a TTL signal sent from Matlab to Arduino to Bonsai.

Running/Resting Recording and Analysis

The mice with optic fiber and headplate were head-fixed on a treadmill. An incremental rotary encoder (Sparkfun, COM-11102) was used to record the speed of the voluntary running. Rotation signal was collected at 25Hz via an Arduino Due board (Arduino, A000062), and digitally sent to Bonsai via serial port communication. All signals are timestamped in Bonsai. Fluorescence lifetime data was collected synchronously at 1 Hz, and video recording to validate running states was simultaneously performed at 25 FPS in Bonsai.

Raw data of running speed was down sampled to 4 Hz for analysis. Running epochs were then defined by continuous forwards or backwards movement above a threshold (1cm/s) for 3 or more seconds. Momentary pausing or slipping on the treadmill can cause single data points in the middle of sustained running to read as 0 cm/s, thus all running epochs were then further analyzed by examining the encoder data point immediately following the running epoch. Running epochs were then extended if this data point showed continued movement (above threshold). Baseline resting periods were defined as continuous below threshold epochs. 30 seconds of "buffer" periods were removed from the beginning and end of the resting epochs to account for ACh return to baseline after movement or any potential preceding ACh rise before running, and the sensor kinetics (point response function) in reaction to these changes. Length of the buffer period was chosen to be longer than necessary to ensure the inclusion of only true resting data. Remaining resting epochs were omitted if shorter than 30 seconds.

ACh activity during running was analyzed by examining photometry data during running epochs, omitting the first second at the beginning of the running epochs to compensate for sensor kinetics. The median value of this period was defined as the sensor reading for each running epoch. The maximum speed during the corresponding epoch was also recorded. This process was repeated for resting epochs. Resting data longer than 30 seconds was also split into 30 second segments to

increase data points. This was repeated for both streams of data (intensity and empirical lifetime). Speed for resting Epochs was defined as 0 and the resulting scatterplots of photometry data vs speed were plotted.

Sleep Stage Scoring

Sleep stages were scored based on the EEG, EMG, and motion detection from the video using a custom-written program written in Python. EEG signals were transformed into a spectrogram. The brain states were scored every 4 seconds semi-automatically using a customized program that performed automatic prediction of sleep states with a random forest model, with the option of user correction and scoring. The following criteria were used to determine sleep/wake stages (Oishi et al., 2016). Active wake: desynchronized EEG, high EMG, and high movement based on video; quiet wakefulness: desynchronized EEG, low EMG, and low movement based on video; NREM sleep: synchronized EEG with high delta power (0.5-4 Hz), low EMG, and low movement based on video; REM sleep: high theta power based on EEG (6-9 Hz), low EMG, and low movement based on video.

Pharmacology

Unless otherwise noted, all chemicals were applied via bath perfusion: they were either added to the perfusion reservoir, orpre-made buffers with the specified chemicals were switched from one to another via a 3-to-1 manifold. Lifetime was allowed to stabilize before a new chemical was added; when there were no clear lifetime changes, 10 minutes were given before the addition of another chemical. The final concentrations of chemicals are specified in brackets: ACh (From 0.001 μM to 100 μM) was from Sigma; cholinesterase inhibitor donepezil hydrochloride (5 μM) was from Sigma; muscarinic acetylcholine receptor antagonist tiotropium bromide was from Tocris; 5-HT (100 μM) was from sigma; dopamine hydrochloride (10 μM) was from Sigma.

For puffing experiments, a glass patch pipette was used to locally puff ACh (200 μM in ACSF) for 3 second onto a neuron in brain slice through a picospritzer (Parker) at 2 psi.

FLIM Simulation

The simulation was done by customized MATLAB code. The null hypothesis is that with or without ACh binding, ACh 3.0 has the same fluorescence lifetime and can be described by the same equation except with higher F_0. The apparent fluorescence lifetime change was solely due to altered proportion of autofluoresence contribution. The fluorescence of ACh 3.0 was modelled by a double exponential decay.

$$F = F_0 \cdot (p_1 \cdot e^{\left(\frac{t}{\tau_1}\right)} + p_2 \cdot e^{\left(\frac{t}{\tau_2}\right)})$$

τ1, τ2, p1 and p2 were determined empirically by measuring the fluorescence decay of ACh 3.0 expressed in HEK cells at saturating concentration of ACh. A large population of photons (~6 x 10^6) with specific lifetimes were generated based on the double exponential decay and binned into 256 time channels over 12.5 ns (time interval between laser pulses for an 80 MHz laser). A small population of photons were sampled from the large population, and the size of photons in the sample correspond to the measured photons at either 0 or 100 μM of ACh respectively. The photon

sample with specified lifetimes were combined with afterpulse (1% of total photon count, with even distribution across lifetime). The histogram generated from the small sample population was then convoluted by a pulse response function. Lifetimes of photons due to autofluorescene were sampled based on empirically determined autofluorescence distribution with imaging of untransfected HEK 293T cells. Lifetimes of photons due to autofluorescence were combined with lifetimes of photons due to the convolved sensor lifetime distribution. Empirical fluorescence lifetime was calculated (as previously described) for each simulated combination and compared to experimental observed values.

Quantification and Statistical Analysis

Detailed information of the quantification and statistics was summarized in the Figure Legends, Figures, and Results. T-test, one-way ANOVA and two-way ANOVA were performed in GraphPad Prism 8. Two-way ANOVA was used to determine the contribution to the total variance from two independent variables. When more than two independent variables were included, stepwise generalized linear model (stepwise GLM) analysis was used to calculate the contribution to the total variance from independent variables. Stepwise GLM was performed in MATLAB and adjust R^2 was calculated as the contribution to the variance. Multinomial logistic regression (MLR) was used to identify the strength of the relationship of individual independent variables (intensity, and lifetime) on states (resting/running; REM/NREM). MLR was performed using scikit-learn library in Python 3. We use f1-scores to identify the accuracy of the logistic regression models and McFadden's pseudo R^2 value to evaluate the fitness of the model. Sample size n refers to biological replicates of number of cells, mice, or behavioral epochs.

Data and Software Availability

The MATLAB programs for ScanImage for data acquisition and analysis are available at https://github.com/YaoChenLabWashU/2pFLIM_acquisition. The MATLAB codes for simulation are available at https://github.com/YaoChenLabWashU/Simulation. The Python codes for analysis of running vs resting behavior are available at https://github.com/YaoChenLabWashU/RvR. The Python programs for sleep staging are available at https://github.com/YaoChenLabWashU/neuroscience_sleep_scoring. All other code is available upon request.

AUTHOR CONTRIBUTIONS

Conceptualization: P.M. and Y.C.; Methodology: P.C., E.T. and Y.C.; Formal Analysis: P.M., P.C., and S.A.; Investigation: P.M., A.O., and Y.C.; Writing: P.M. and Y.C.; Visualization: P.M., A.O. and Y.C.; Supervision: Y.C.; Funding Acquisition: Y.C.

ACKNOWLEDGEMENTS

We thank Yulong Li and lab for sharing plasmids of neuromodulator sensors and for discussions. We thank Sophie Ma for validation of sleep scoring results. We thank Adam Kepecs, Meaghan Creed, and the labs of Yao Chen, Tim Holy, and Daniel Kerschensteiner for helpful feedback. Funding for this work was supported by the U.S. National Institute of Neurological Disorders and Stroke (R01 NS119821, to Y.C.), the Whitehall Foundation (2019-08-64, to Y.C.), a gift

from the Howard Hughes Medical Institute (to Y.C.), and the McDonnell International Scholars Academy of Washington University in St. Louis (to P.M.)

DECLARATION OF INTERESTS

The authors declare no competing interests.

REFERENCES

Arbuthnott, G.W., and Wickens, J. (2007). Space, time and dopamine. Trends Neurosci. *30*, 62–69.

Bargmann, C.I., and Marder, E. (2013). FOCUS ON MAPPING THE BRAIN From the connectome to brain function. Nat. Methods *10*, 438–490.

Becker, W., and Bergmann, A. (2002). Lifetime imaging techniques for optical microscopy. Becker & Hickl GmbH,. Berlin 1–41.

Borden, P.M., Zhang, P., Shivange, A. V, Marvin, J.S., Cichon, J., Dan, C., Podgorski, K., Figueiredo, A., Novak, O., Tanimoto, M., et al. (2020). A Fast Genetically Encoded Fluorescent Sensor for Faithful *in vivo* Acetylcholine Detection in Mice, Fish, Worms and Flies. SSRN Electron. J.

Brinks, D., Klein, A.J., and Cohen, A.E. (2015). Two-Photon Lifetime Imaging of Voltage Indicating Proteins as a Probe of Absolute Membrane Voltage. Biophys. J. *109*, 914.

Chen, Y., and Sabatini, B.L. (2012). Signaling in dendritic spines and spine microdomains. Curr. Opin. Neurobiol. *22*, 389–396.

Chen, Y., Saulnier, J.L., Yellen, G., and Sabatini, B.L. (2014). A PKA activity sensor for quantitative analysis of endogenous GPCR signaling via 2-photon FRET-FLIM imaging. Front. Pharmacol. *5*, 56.

Chen, Y., Granger, A., Tran, T., Saulnier, J.L., Kirkwood, A., and Sabatini, B.L. (2017). Endogenous Gαq-coupled neuromodulator receptors activate protein kinase A. Neuron *96*, 1070-1083.e5.

Dong, C., Zheng, Y., Long-Iyer, K., Wright, E.C., Li, Y., and Tian, L. (2022). Fluorescence Imaging of Neural Activity, Neurochemical Dynamics, and Drug-Specific Receptor Conformation with Genetically Encoded Sensors. Annu. Rev. Neurosci. *45*, 273–294.

Feng, J., Zhang, C., Lischinsky, J.E., Jing, M., Zhou, J., Wang, H., Zhang, Y., Dong, A., Wu, Z., Wu, H., et al. (2019). A Genetically Encoded Fluorescent Sensor for Rapid and Specific In Vivo Detection of Norepinephrine. Neuron *102*, 745-761.e8.

Ganesana, M., Lee, S.T., Wang, Y., and Venton, B.J. (2017). Analytical Techniques in Neuroscience: Recent Advances in Imaging, Separation, and Electrochemical Methods. Anal. Chem. *89*, 314–341.

Jensen, K.R., Berthoux, C., Nasrallah, K., and Castillo, P.E. (2021). Multiple cannabinoid signaling cascades powerfully suppress recurrent excitation in the hippocampus. Proc. Natl. Acad. Sci. U. S. A. *118*.

Jing, M., Zhang, P., Wang, G., Feng, J., Mesik, L., Zeng, J., Jiang, H., Wang, S., Looby, J.C., Guagliardo, N.A., et al. (2018). A genetically encoded fluorescent acetylcholine indicator for in vitro and in vivo studies. Nat. Biotechnol.

Jing, M., Li, Y., Zeng, J., Huang, P., Skirzewski, M., Kljakic, O., Peng, W., Qian, T., Tan, K., Zou, J., et al. (2020). An optimized acetylcholine sensor for monitoring in vivo cholinergic

activity. Nat. Methods *17*.

Lakowicz, J.R., Szmacinski, H., and Johnson, M.L. (1992). Calcium Imaging Using Fluorescence Lifetimes and Long-Wavelength Probes. J. Fluoresc. *2*, 47.

Lazzari-Dean, J.R., Gest, A.M.M., and Miller, E.W. (2019). Optical estimation of absolute membrane potential using fluorescence lifetime imaging. Elife *8*.

Lee, S.J., Chen, Y., Lodder, B., and Sabatini, B.L. (2019). Monitoring Behaviorally Induced Biochemical Changes Using Fluorescence Lifetime Photometry. Front. Neurosci. *13*, 766.

van der Linden, F.H., Mahlandt, E.K., Arts, J.J.G., Beumer, J., Puschhof, J., de Man, S.M.A., Chertkova, A.O., Ponsioen, B., Clevers, H., van Buul, J.D., et al. (2021). A turquoise fluorescence lifetime-based biosensor for quantitative imaging of intracellular calcium. Nat. Commun. 2021 121 *12*, 1–13.

Marder, E. (2012). Neuromodulation of Neuronal Circuits: Back to the Future. Neuron *76*, 1–11.

McCall, J.G., Al-Hasani, R., Siuda, E.R., Hong, D.Y., Norris, A.J., Ford, C.P., and Bruchas, M.R. (2015). CRH Engagement of the Locus Coeruleus Noradrenergic System Mediates Stress-Induced Anxiety. Neuron *87*, 605–620.

Mongeon, R., Venkatachalam, V., and Yellen, G. (2016). Cytosolic NADH-NAD(+) Redox Visualized in Brain Slices by Two-Photon Fluorescence Lifetime Biosensor Imaging. Antioxid. Redox Signal. *25*, 553–563.

Oishi, Y., Takata, Y., Taguchi, Y., Kohtoh, S., Urade, Y., and Lazarus, M. (2016). Polygraphic recording procedure for measuring sleep in mice. J. Vis. Exp. *2016*, 53678.

Parikh, V., Kozak, R., Martinez, V., and Sarter, M. (2007). Prefrontal Acetylcholine Release Controls Cue Detection on Multiple Timescales. Neuron *56*, 141–154.

Patriarchi, T., Cho, J.R., Merten, K., Howe, M.W., Marley, A., Xiong, W.H., Folk, R.W., Broussard, G.J., Liang, R., Jang, M.J., et al. (2018). Ultrafast neuronal imaging of dopamine dynamics with designed genetically encoded sensors. Science *360*.

Pologruto, T.A., Sabatini, B.L., and Svoboda, K. (2003). ScanImage: flexible software for operating laser scanning microscopes. Biomed. Eng. Online *2*, 13.

Puthongkham, P., Analyst, B.V.-, and 2020, undefined Recent advances in fast-scan cyclic voltammetry. Pubs.Rsc.Org.

Sabatini, B.L., and Tian, L. (2020). Imaging Neurotransmitter and Neuromodulator Dynamics In Vivo with Genetically Encoded Indicators. Neuron *108*, 17–32.

Schmack, K., Bosc, M., Ott, T., Sturgill, J.F., and Kepecs, A. (2021). Striatal dopamine mediates hallucination-like perception in mice. Science *372*.

Sun, F., Zhou, J., Dai, B., Qian, T., Zeng, J., Li, X., Zhuo, Y., Zhang, Y., Wang, Y., Qian, C., et al. (2020). Next-generation GRAB sensors for monitoring dopaminergic activity in vivo. Nat. Methods *17*, 1156.

Ting, J.T., Lee, B.R., Chong, P., Soler-Llavina, G., Cobbs, C., Koch, C., Zeng, H., and Lein, E.

(2018). Preparation of Acute Brain Slices Using an Optimized N-Methyl-D-glucamine Protective Recovery Method. J. Vis. Exp. 53825.

Tuveson, D. a., Shaw, A.T., Willis, N. a., Silver, D.P., Jackson, E.L., Chang, S., Mercer, K.L., Grochow, R., Hock, H., Crowley, D., et al. (2004). Endogenous oncogenic K-rasG12D stimulates proliferation and widespread neoplastic and developmental defects. Cancer Cell *5*, 375–387.

Ungerstedt, U., sciences, Å.H.-L., and 1987, undefined In vivo microdialysis-a new approach to the analysis of neurotransmitters in the brain. Elsevier.

Venton, B., Analyst, Q.C.-, and 2020, undefined Fundamentals of fast-scan cyclic voltammetry for dopamine detection. Pubs.Rsc.Org.

Wan, J., Peng, W., Li, X., Qian, T., Song, K., Zeng, J., Deng, F., Hao, S., Feng, J., Zhang, P., et al. (2021). A genetically encoded sensor for measuring serotonin dynamics. Nat. Neurosci. *24*, 746–752.

Watabe-Uchida, M., Eshel, N., and Uchida, N. (2017). Neural Circuitry of Reward Prediction Error. Annu. Rev. Neurosci. *40*, 373–394.

Wightman, R.M. (2006). Probing cellular chemistry in biological systems with microelectrodes. Science (80-.). *311*, 1570–1574.

Wu, Z., Lin, D., and Li, Y. (2022). Pushing the frontiers: tools for monitoring neurotransmitters and neuromodulators. Nat. Rev. Neurosci. *23*, 257–274.

Yasuda, R. (2006). Imaging spatiotemporal dynamics of neuronal signaling using fluorescence resonance energy transfer and fluorescence lifetime imaging microscopy. Curr. Opin. Neurobiol. *16*, 551–561.

Zheng, K., Bard, L., Reynolds, J.P., King, C., Jensen, T.P., Gourine, A. V., and Rusakov, D.A. (2015). Time-Resolved Imaging Reveals Heterogeneous Landscapes of Nanomolar Ca2+ in Neurons and Astroglia. Neuron *88*, 277–288.

Zheng, K., Jensen, T.P., and Rusakov, D.A. (2018). Monitoring intracellular nanomolar calcium using fluorescence lifetime imaging. Nat. Protoc. 2018 133 *13*, 581–597.

FIGURE LEGENDS

Figure 1. Screening fluorescence lifetime changes of neuromodulator sensors reveals lifetime response in the ACh sensor GRAB-ACh3.0. (A) Neuromodulator sensors show fluorescence intensity increase, but it is unclear whether they show any fluorescence lifetime change. **(B)** Fluorescence Intensity and lifetime changes of different neuromodulator sensors in response to saturating concentrations of the corresponding neuromodulators in 293T cells (GRAB-ACh3.0 n = 13, iAchSnFR n = 11,GRAB-DA2h n = 4, dLight1.1 n = 9, GRAB-NE n = 6, GRAB-5-HT n =9. $^{*}p < 0.05$ from t-test vs baseline change). **(C)** Fluorescence lifetime decays of ACh sensor under baseline and saturating ACh conditions (100 μM). **(D-G)** Representative images (D, F) and traces (E, G) showing fluorescence intensity (D, E) or lifetime (F, G) of the ACh sensor GRAB-ACh3.0 in response to saturating concentration of ACh (100 μM), muscarinic ACh receptor (mAChR) antagonist Tiotropium (Tio, 5 μM), or ACh and Tio in HEK 293T cells. The trace in E and G shows the response of the cell denoted by a triangle in D and F. **(H)** Summary of the traces of normalized intensity and fluorescence lifetime change of ACh sensor showing their response to ACh and mAChR antagonist Tio. (n = 8). Data shows mean±SEM. **(I)** Summary data of the fluorescence lifetime and intensity changes of ACh sensor in HEK 293T cells (n = 13). $^{**}p < 0.01$ vs Baseline; $^{\#\#}p < 0.01$ vs ACh from one-way ANOVA.

Figure 2. Simulation reveals that the observed fluorescence lifetime change of ACh sensor is authentic. **(A)** Schematic illustrating how fluorescence intensity increase without lifetime change of the sensor could lead to observed fluorescence lifetime increase due to more sensor contribution to lifetime calculation compared with autofluorescence. **(B)** Lifetime decay curves of HEK293T cells with no sensor transfection and cells expressing GRAB-ACh3.0 (with 100 μM ACh). The inset shows their normalized fluorescence lifetime decay curves, indicating that the lifetime of autofluorescence is shorter than sensor fluorescence. **(C)** Fluorescence lifetime distribution of GRAB-ACh3.0 sensor from simulation (n = 50 for both low and high photon count) or actual experiments. Experimental data were collected in the absence or presence of ACh (100 μM). Simulation assumes only intensity change, and no lifetime change of the fluorescence sensor.

Figure 3. Fluorescence lifetime of GRAB-ACh3.0 is dose-sensitive and responds to transient ACh in brain tissue (A) Sample traces (left) and summary data (right) showing the dose-dependent response of both intensity (upper panels) and fluorescence lifetime (lower panels) change of GRAB-ACh3.0 in HEK 293T cells (n = 6, data shows median+/-interquartile). **(B, C, D)** Example heatmap (B), trace (C), and summary data (D) showing the intensity and fluorescence lifetime changes of GRAB-ACh3.0 expressed in hippocampus CA1 pyramidal neuronsin response to two concentrations of ACh and the mAChR antagonist Tiotropium (5 μM). N = 9 from 3 mice, data shows mean+/-SEM. **(E)** Image showing puffing of ACh onto a CA1 pyramidal neuron. **(F, G)** Example traces and summary data showing intensity and fluorescence lifetime responses of GRAB-ACh3.0 to ACh (200 μM). $^{*}p < 0.05$, $^{**}p < 0.01$ vs Baseline; $^{\#\#}p < 0.01$ vs ACh from one-way ANOVA. N = 11 from 3 mice, data shows mean+/-SEM.

Figure 4. Fluorescence lifetime measurement is stable across different excitation light powers. **(A)** Representative traces of intensity (left) and fluorescence lifetime (right) changes of GRAB-ACh3.0 imaged at different laser powers in 293T cells. **(B,C)** Summary data (left) and two-way ANOVA analysis (right) of intensity (B) and fluorescence lifetime (C) measurement of GRAB-ACh3.0 under different laser powers. Two-way ANOVA analysis shows the contribution to the total variance of the measurements due to ACh concentration, laser power, or cell identity. Note that for fluorescence lifetime measurement, ACh condition was the only major contributor to the total variance. Each circle represents data from a single cell. N = 15. Line and error bars indicate mean+/-SEM.

Figure 5 Fluorescence lifetime measurement of GRAB-ACh3.0 accurately predicts running vs resting across imaging laser powers and across mice. (A) Adeno-associated virus carrying Cre-dependent GRAB-ACh3.0 was delivered to CA1 cells in the hippocampus of Emx1^{IREScre} *mice.* Fluorescence lifetime photometry (FLiP) was performed as head-fixed mice ran or rested on a treadmill. **(B)** Example traces showing fluorescence lifetime (upper panel) and intensity (intensity) increase in GRAB-ACh3.0-expressing mice from resting to running. **(C)** Distribution of fluorescence lifetime and intensity measurements of GRAB-ACh3.0 from the same mouse but under different laser powers. Fluorescence lifetime or intensity were calculated from the median of each running or resting epoch (laser power 1: resting n =26; running n = 31. Laser power 2: resting n = 38; running n = 6). **(D)** Distribution of fluorescence lifetime and intensity measurements of GRAB-ACh3.0 under the same laser power from different mice. Mouse 1: resting n= 25, running n = 28; mouse 2: resting = 31, running n = 17; mouse 3: resting = 6, running n = 43; mouse 4: resting = 10, running n = 35. **(E)** Distribution of fluorescence lifetime and intensity measurements of GRAB-ACh3.0 across running and resting states, pooled from all mice across different laser powers (14 recordings from 7 mice under 3 different laser powers). N=326 for resting; n=465 for running. **(F)** Results from stepwise generalized linear model (GLM) analysis showing the contribution to the total variance of lifetime or intensity from behavior states, laser power, and animal identities. Total adjusted R^2 from GLM: fluorescence lifetime 0.9178 and intensity 0.995. **(G)** Multinomial logistic regression (MLR) analysis showing the F1 score of predicting running or resting state using either fluorescence lifetime or intensity measurements of GRAB-ACh3.0, regardless of the imaging laser powers and animal identities (pseudo-R2 from MLR analysis: fluorescence lifetime 0.72 and intensity 0.02). Each circle represents a running or resting epoch. Line and error bars show median+/-interquartile. **p < 0.01 from two-way ANOVA or t-test.

Figure 6 Fluorescence lifetime of GRAB-ACh3.0 predicts sleep-wake states accurately across long weeks and animals. **(A)** Illustration showing experimental setup. Following viral delivery of GRAB-ACh3.0 to hippocampal CA1 region of Emx1^{IREScre} *mice, fluorescence lifetime photometry (*FLiP) was performed along with EEG/EMG and video recordings across sleep-wake cycles. **(B)** One hour of representative spectrogram of EEG trace, EMG trace, the corresponding scored sleep-wake states, along with fluorescence lifetime and intensity traces from a mouse,

showing increase in GRAB-ACh3.0 intensity and lifetime during REM and active wakefulness. **(C)** Distribution of the fluorescence lifetime and intensity measurements of GRAB-ACh3.0 sensor in different sleep-wake states from a 12-hour FLiP recording of one mouse. Each data point shows the median during a sleep or wake state epoch. N = 69, 28, 54, 16 for active wake (AW), quiet wake (QW), NREM, and REM respectively. **(D)** Representative trace of fluorescence lifetime and intensity measurements of GRAB-ACh3.0 in NREM. Recordings were performed at different time points after virus injection. Note that fluorescence lifetime measurement from the same state was stable over time while the intensity showed major increase over time. **(E)** Summary (left) and two-way ANOVA analysis (right) of fluorescence lifetime or intensity of ACh sensor in different sleep-wake states in one mouse across time. (3 weeks: n = 56, 13, 53, 27 epochs; 6 weeks: n = 48, 8, 63, 32 epochs; 8 weeks: n = 69, 28, 54, 16 epochs, for AW, QW, NREM, and REM stages). Two-way ANOVA analysis shows the relative contribution to the total variance of lifetime or intensity by behavior states (NREM versus REM) or time since viral delivery (n = 7 mice). **(F)** Summary (left) and two-way ANOVA analysis (right) of fluorescence lifetime or intensity of ACh sensor in different sleep-wake states at one time point across mice. (n=7 mice). Two-way ANOVA analysis shows the relative contribution to the total variance of lifetime or intensity by behavior states (NREM versus REM) or animal identity (n = 3 time points). **(G)** Stepwise GLM analysis results showing the contribution to the total variance of lifetime or intensity measurements from behavior states (NREM vs REM), time since sensory delivery, or animal identities. **(H)** Multinomial logistic regression (MLR) analysis resulting showing F1 score reporting how accurately NREM versus REM states can be predicted with fluorescence lifetime or intensity data of GRAB-ACh3.0 ((pseudo-R2 from MLR analysis: fluorescence lifetime 0.52 and intensity 0.01).). Each data point represents a behavior epoch. Graphs show median+/-interquartile.

Figure 1

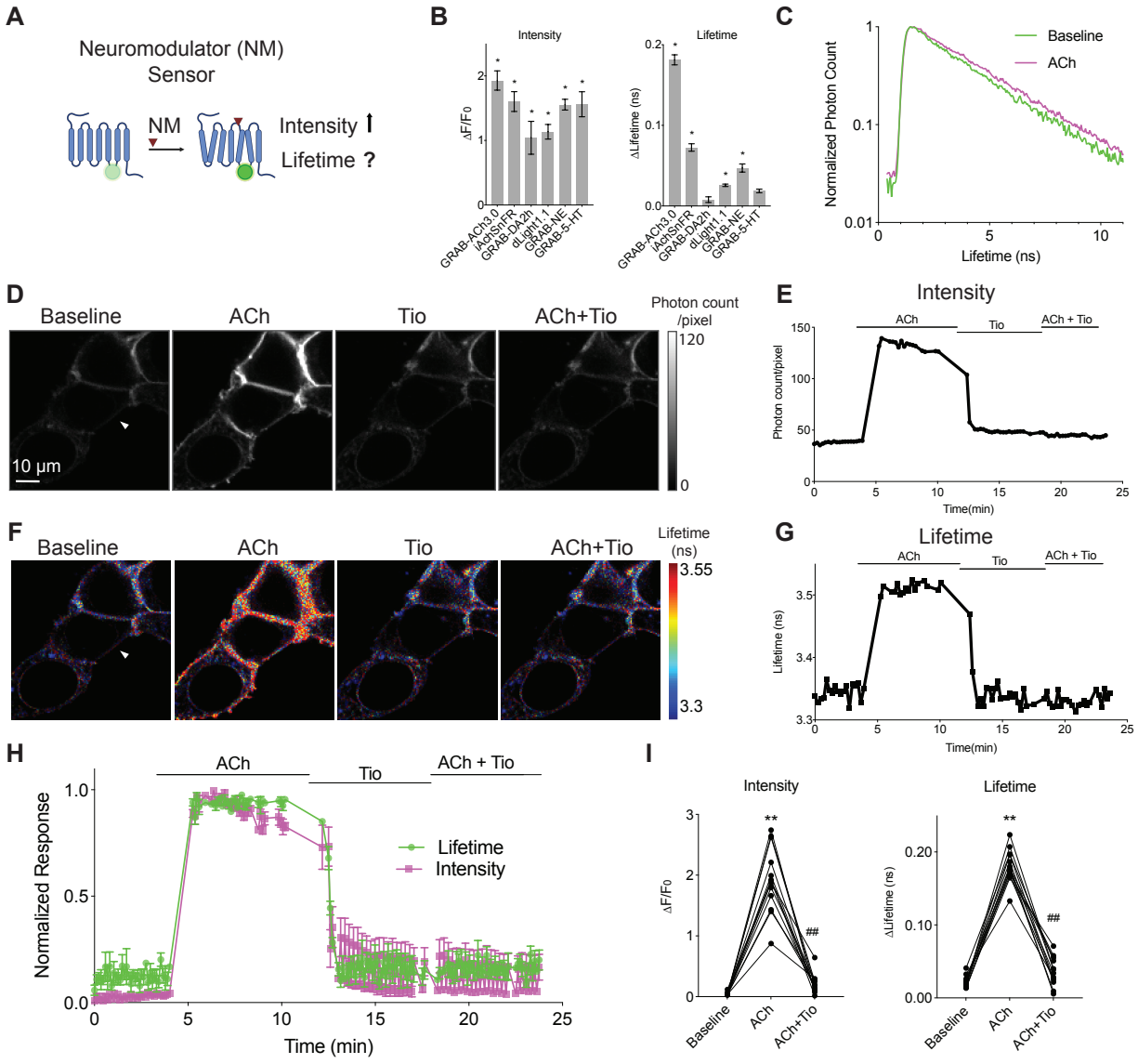

Figure 2

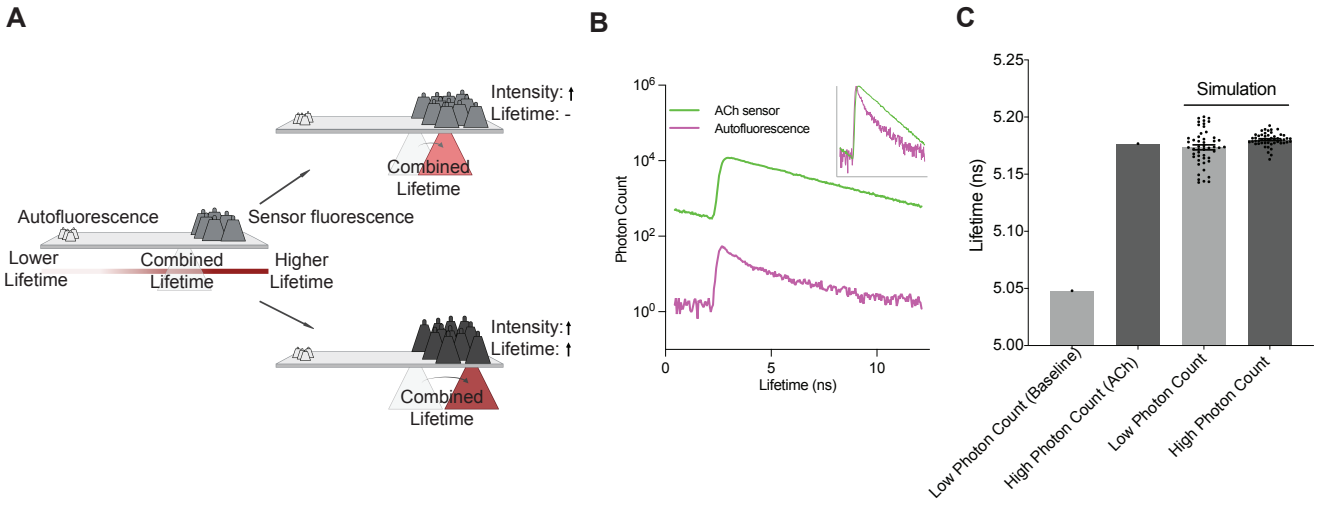

Figure 3

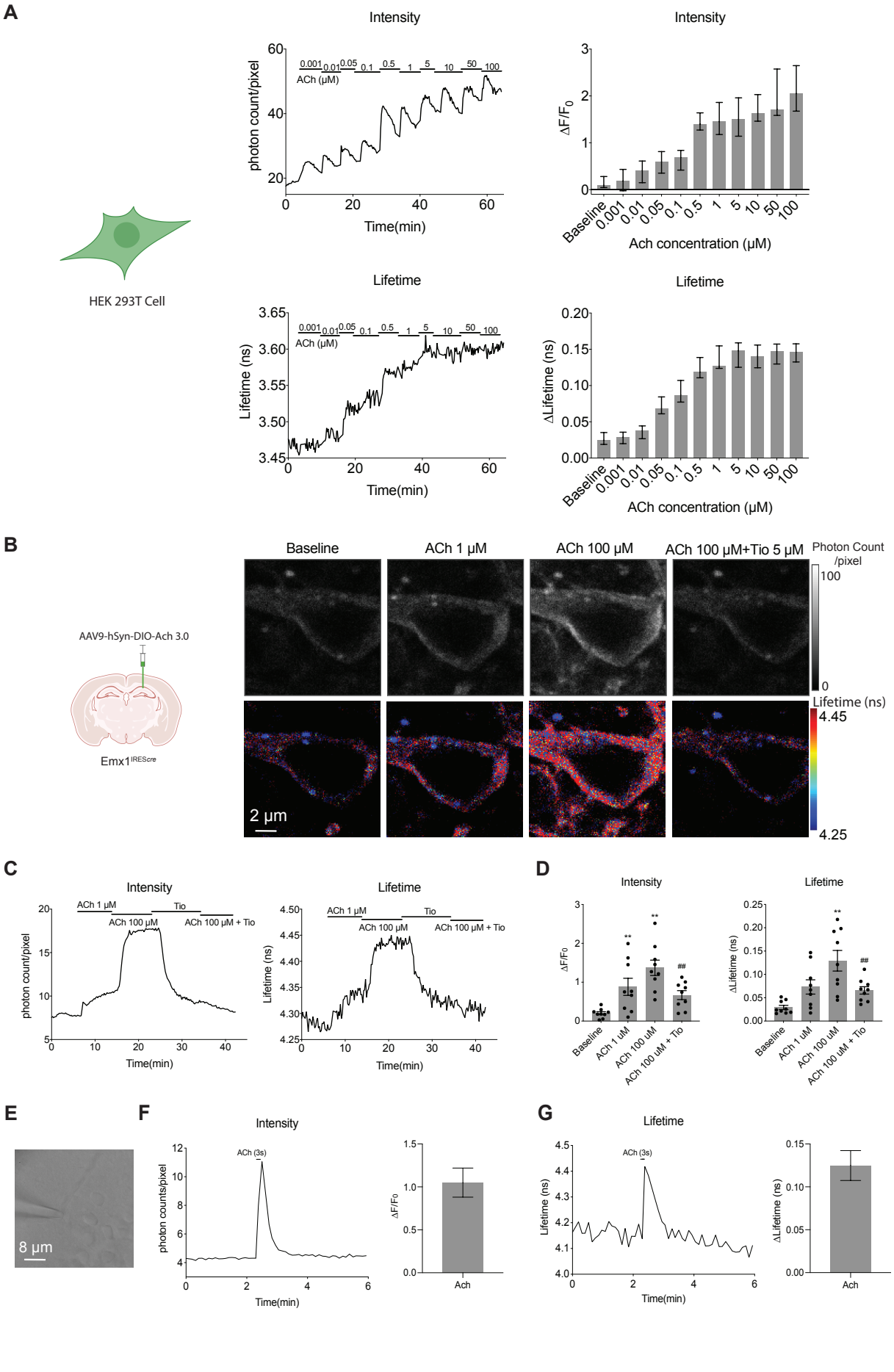

Figure 4

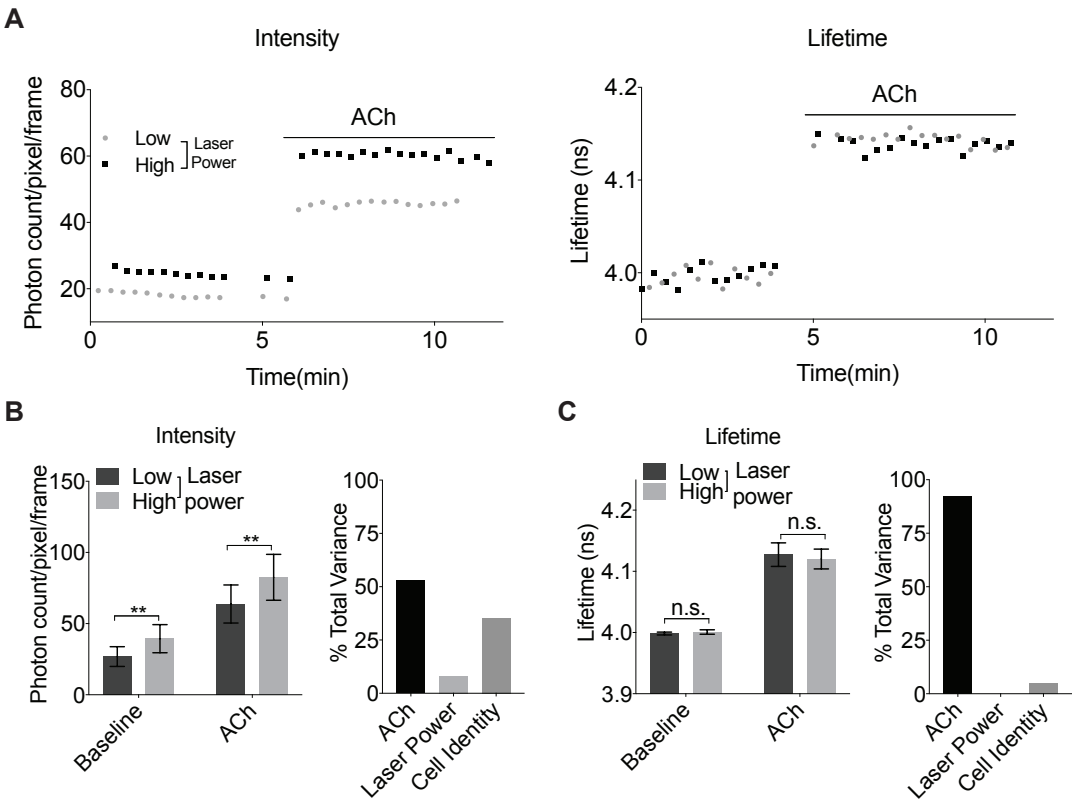

Figure 5

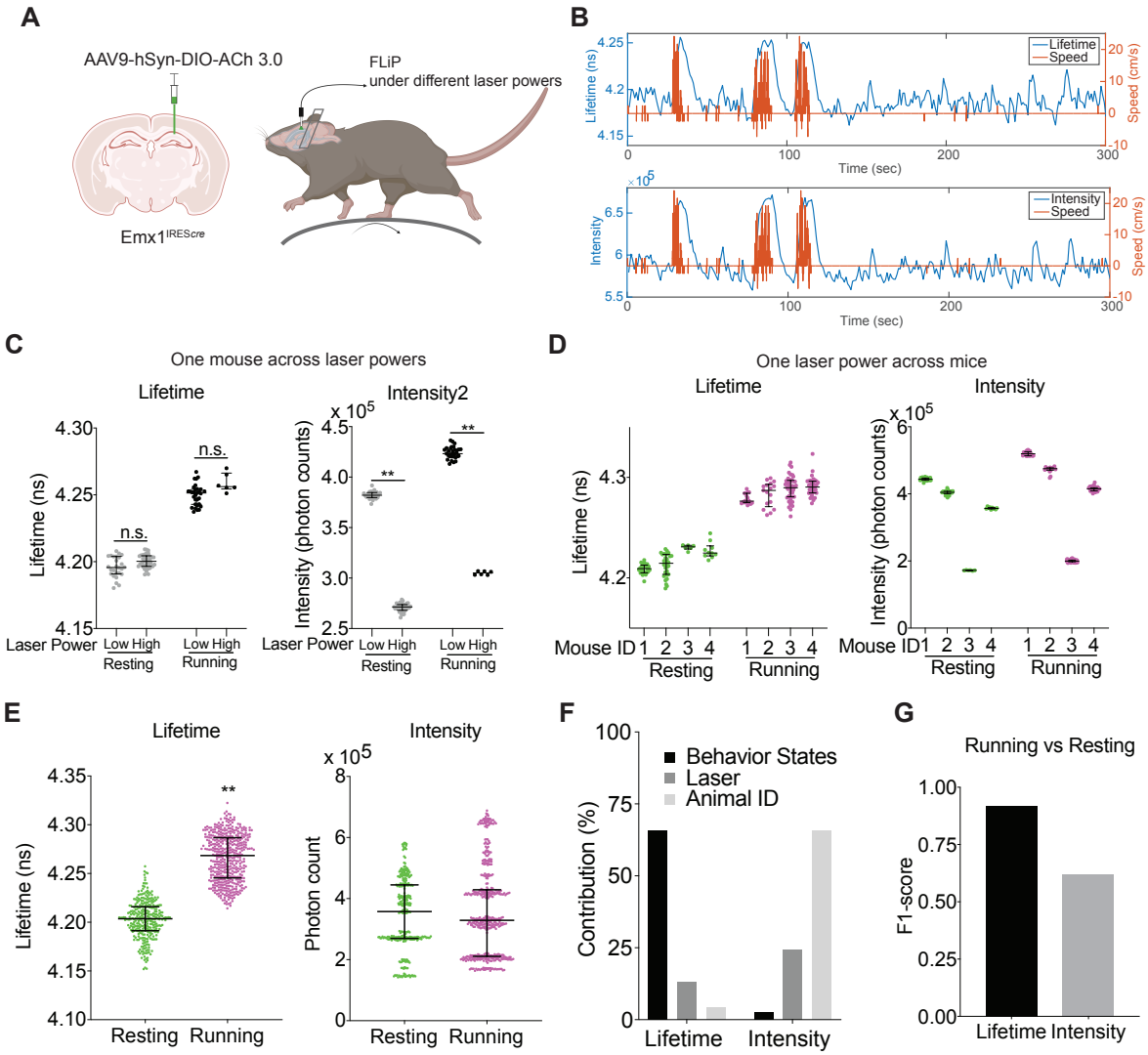

Figure 6